Vibrational dynamics of large hot molecules in the collisionless gas phase

C. Stromberg, D. J. Myers, and M. D. Fayer
Department of Chemistry, Stanford University, Stanford, California 94305

(Received 26 September 2001; accepted 6 December 2001)

Infrared ps pump-probe experiments are presented for the *P*, *Q*, and *R* rotational branches of the asymmetric CO stretching mode of tungsten hexacarbonyl (1997 cm^{-1}) in the collisionless gas phase. The pump-probe decays are tri-exponentials (140 ps, 1.3 ns, and >100 ns) in contrast to single exponential decays observed in supercritical fluids and liquid solvents. The 1.3 ns decay component is the vibrational energy relaxation (VER) time. The long component occurs following intramolecular VER into a distribution of low-frequency modes. After VER is complete, the *R* signal is 48%, the *Q* signal is 29%, and the *P* signal is −10% (absorption increase) compared to the $t=0$ signal. These long-lived signals result from an increase in the occupation numbers of low-frequency modes (internal heating) that causes a shift of the vibrational spectrum. The fastest decay is produced by spectral diffusion. The spectrally narrow pump pulse burns a hole in the inhomogeneous ground state spectrum and generates a narrow spectral population in the excited state (excited state peak). The inhomogeneity arises from the distribution of occupation numbers of the low-frequency modes that produces different combination band spectral shifts. Spectral diffusion is caused by the time evolution of the complex low-frequency thermal vibrational wave packet. Two possible models for the spectral diffusion are evaluated, one in which spectral diffusion reduces the pump-probe signal by hole filling and broadening of the excited state peak, and one in which the spectral diffusion only broadens the excited state peak.
[DOI: 10.1063/1.1446850]

I. INTRODUCTION

Vibrational energy relaxation (VER) is important in a wide variety of processes ranging from electron transfer[1,2] to shock-induced chemistry.[3] In the gas phase, VER is intimately involved in chemical reactions.[4] In spite of its importance and a great deal of theoretical[5–11] and experimental effort,[12–21] the dynamics of vibrations, particularly in complex polyatomic molecules, are not well understood. In condensed phases, a diatomic molecule in an atomic solvent can only undergo VER by transferring vibrational energy to the translational degrees of freedom of the solvent. VER in a pure diatomic liquid, such as N_2 or O_2, can involve transfer of vibrational energy to rotational as well as translational degrees of freedom. VER in polyatomic molecules in condensed matter systems can occur through these pathways, as well as through pathways not available in diatomic systems. If a high-frequency vibration is excited, it can relax by a combination of intra- and intermolecular pathways.[5,6] VER of a high-frequency mode can occur by excitation of a number of lower frequency intramolecular modes plus excitation of one or more quanta of the continuum of bath modes that permit conservation of energy.[5] VER of diatomics either pure or in atomic solvents can be extremely slow because a large number of quanta of the bath must be simultaneously excited,[22–24] while VER of polyatomics can be rapid because a combination of only a small number of internal modes plus one or a small number of bath quanta need to participate in the relaxation process.[5,25]

In the gas phase, diatomic molecules or small polyatomic molecules (density of states less than about 10 states per cm^{-1}) require collisions to undergo VER.[26] A small molecule will have an insufficient density of low-frequency states to provide an intramolecular VER route that conserves energy. For either a diatomic or small polyatomic molecule, collisions provide a mechanism through which energy can be conserved. However, a moderately sized polyatomic molecule, with many low-frequency modes, can undergo collisionless intramolecular VER because the high density of low-frequency states provides an essentially continuous intramolecular bath into which the energy of an excited high-frequency mode can relax.[18]

In this article, experiments are presented that examine vibrational dynamics following infrared excitation of a single vibrational quantum of a high-frequency mode of a moderate size molecule, tungsten hexacarbonyl [$W(CO)_6$], at elevated temperature (326 K) in the collisionless gas phase. Following excitation of the asymmetric stretching mode (T_{1u} mode) at ~2000 cm^{-1}, the vibrational dynamics are observed as a function of time with a delayed probe pulse. IR pump-probe experiments on the T_{1u} mode of $W(CO)_6$ have been performed in several supercritical fluids[19,20,27,28] and in a number of liquid solvents.[14] In the SCF and liquid solvents, the vibrational pump-probe decays are single exponentials. In liquids, orientational relaxation can give rise to a nonexponential decay.[29] However, if the probe is set at the magic angle, the population relaxation is a single exponential.[29] In one set of experiments, in which the IR bandwidth was small compared to the inhomogeneously broadened absorption line in the liquid and glassy states, spectral diffusion caused the pump-probe decays to be biexponential.[29]

In the experiments presented below on the T_{1u} mode of

$W(CO)_6$ in the collisionless gas phase, the pump-probe decays were measured on the *P, Q,* and *R* rotational branches. In all cases, the decays are triexponentials.[18] The three components are 140 ps, 1.3 ns, and >100 ns. Extrapolation of density-dependent pump-probe measurements in SCF solvents shows that the 1.3 ns decay is the VER. On the maximum time scale of the experiments (12 ns), the longest decay component appears as a plateau. The level of the plateau is different for the *P, Q,* and *R* branches. After VER is complete, the *R* signal is 48%, the *Q* signal is 29%, and the *P* signal is -10% (absorption increase) compared to the $t=0$ signal.

A theoretical model is developed that is able to semiquantitatively reproduce the observations. To reproduce the absorption spectrum, it is necessary to include inhomogeneous broadening of each thermally populated rotational state of the vibrational transition. Inhomogeneous broadening is usually associated with condensed phase systems in which a distribution of local solvent environments causes small changes in the vibrational frequency. In the collisionless gas phase at very low temperatures (supersonic molecular beam), vibrational transitions will be homogeneously broadened except for a small amount of residual Doppler broadening. However, it has been recognized for some time that at elevated temperatures, thermal population of low-frequency modes of moderate to large size molecules can cause anomalous ''hot band'' broadening of vibrational transitions.[30]

A moderate-sized molecule, like $W(CO)_6$, at elevated temperatures is fundamentally different from a very cold molecule. $W(CO)_6$ has a large number of low-frequency modes between $\sim$100 and 600 cm^{-1}. At elevated temperatures, these modes are thermally populated. Since the normal modes of $W(CO)_6$ are well known, the average thermal energy in $W(CO)_6$ at the experimental temperature can be calculated, within the harmonic approximation. The resultant average thermal energy is 2900 cm^{-1}, and the spread in energy about the average is very broad.[18,31,32] At any given time, a particular molecule will have some set of mode occupation numbers that make up the internal energy of the molecule. The ensemble of molecules has a broad distribution of sets of occupation numbers. Molecules will have different internal energies, and, therefore, different vibrational occupation numbers. However, even molecules with virtually identical total vibrational energies can have a wide variety of sets of occupation numbers because of the high density of populated vibrational states at elevated temperatures. The different sets of occupation numbers in different molecules will lead to slightly different transition frequencies, because of T_{lu} mode combination band shifts that depend on the occupation numbers of other modes. The result is inhomogeneous broadening of the spectrum. The extent of the inhomogeneous broadening is obtained by careful modeling of the experimental absorption spectrum.

In the time-dependent experiments, the IR pump and probe pulses have narrow bandwidths compared to the inhomogeneous linewidth. The pump pulse excites only a fraction of the molecules. A relatively narrow hole is ''burned'' in the ground state population and a correspondingly narrow excited state peak is generated. The inhomogeneous broadening discussed above is not static, however. Each molecule is in a superposition of vibrational states that was prepared by the last collision prior to the measurement. Each state has associated with it a time-dependent phase factor. The superposition is a complex vibrational wave packet that is evolving in time. The time dependence of the wave packet causes a time-dependent evolution in the transition frequency of a given molecule. Time-dependent shifts in transition frequencies are commonly observed in condensed matter systems.[29,33,34] The time evolution of the transition frequency is called spectral diffusion. The overall effect for the ensemble of gas phase molecules can be filling of the ground state hole and spreading of the excited state peak, or possibly only spreading of the excited state peak depending on the model used for the spectral diffusion. Filling of the hole reduces ground state bleaching and spreading of the peak reduces stimulated emission; both decrease the signal measured by the delayed probe pulse. As discussed in detail below, the fast component of the pump-probe signal decay ($\sim$ 140 ps) is caused by spectral diffusion.

Following VER (1.3 ns), the system does not immediately return to its initial conditions. There is a very long-lived component to the pump-probe signal. The VER eliminates the stimulated emission contribution to the pump-probe signal (50% of the signal). In the absence of collisions, the $\sim$2000 cm^{-1} of T_{lu} vibrational energy remains in the low-frequency modes of the molecule. This energy produces a significant increase in the occupation numbers of the low-frequency modes. The increase in vibrational energy in the low-frequency modes produces a redshift of the spectrum for the molecules that undergo VER. The redshift influences the observed magnitude of the ground state recovery (decrease in bleaching). Pumping and probing on the *R* branch produces the smallest drop in signal because the spectrum shifts to the red, moving the relevant components of the spectrum away from the probe wavelength. In the *Q* branch, the spectrum shifts the same amount, but in this case there is more ground state recovery as a portion of the *R* branch shifts onto the probe pulse. Pumping and probing on the *P* branch (red side of the spectrum) produces a negative signal (more absorption than prior to pumping) because the redshift results in the probe wavelength sampling a part of the spectrum that is more strongly absorbing than initially. The observations of the long-lived pump-probe signals are semi-quantitatively described by the theoretical model that involves a single value for the magnitude of the redshift in the spectrum following VER. The size of the redshift demonstrates that VER does not produce a thermalized distribution of low-frequency modes in the absence of collisions.

In the following, data and a detailed model are presented that explicate the issues introduced above. The fundamental question is how should large, hot molecules in the collisionless gas phase be viewed? The picture that immerges is one of an inhomogeneous ensemble of molecules that is undergoing substantial dynamics even in the absence of collisions. Inhomogeneity and hole burning are generally associated with molecules in condensed matter systems.[34] The results of the experiments show that large hot gas phase molecules can

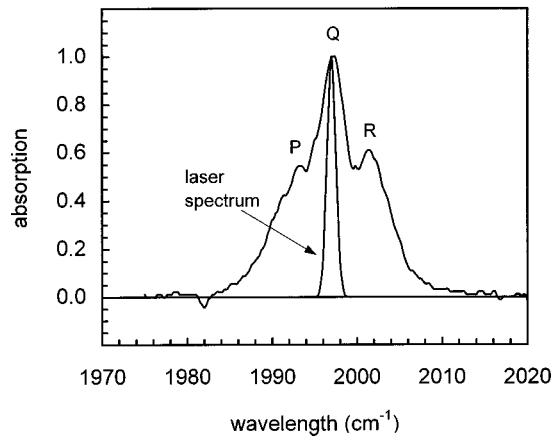

FIG. 1. An FT-IR spectrum of the T_{lu} CO stretching mode of $W(CO)_6$ in the gas phase. The *P*, *Q*, and *R* rotational branches are visible in the spectrum. The laser line, centered at 1997 cm^{-1}, is also shown for comparison.

exhibit behavior that, in many respects, is similar to molecules in condensed phases.

II. EXPERIMENTAL PROCEDURES

Infrared vibrational pump-probe experiments (transient absorption measurements) were conducted on four wavelengths within the asymmetric CO stretching mode (T_{lu}) of gas phase $W(CO)_6$. The doubled output of a mode-locked, *Q*-switched and cavity dumped Nd:YAG laser was used to both pump a dye laser and as the pump pulse in an optical parametric amplifier (OPA). The IR pulse train that emerges from the YAG output coupler is double and used to synchronously pump the dye laser, which is cavity dumped (~40 ps pulses). The YAG laser is also cavity dumped. The resulting IR pulse is doubled, and the residual IR pulse is also doubled. The 532 nm light made from the residual IR pulse pumps a double-pass dye amplifier cell. The main doubled cavity dumped pulse is the pump pulse in a $LiIO_3$ OPA. The amplified dye pulse is the signal in the OPA. The idler generated in the OPA provides the tunable IR. The frequency of the IR is tuned by tuning the dye laser, using etalons, to different wavelengths across the absorption spectrum of the $\nu=0\rightarrow1$ CO T_{lu} mode. The OPA output is ~1 μJ. The pulse spectrum is well fit by a Gaussian with a sigma of 0.515 cm^{-1} (1.21 cm^{-1} FWHM).

The sample was made by placing a small amount of $W(CO)_6$ solid in a stainless steel cell with CaF_2 windows. The cell was then evacuated to the point that the vapor pressure of the $W(CO)_6$ was the limiting pressure. The cell was sealed and heated to 50 °C to produce enough vapor pressure to conduct the experiment. The pressure is so low that the average collision time (~1 μs) is many orders of magnitude longer than the time scale of the measurements. FT-IR spectra of the sample displayed *P*, *Q*, and *R* rotational branches. The *P* branch was centered at 1993.3 cm^{-1}, the *Q* branch was centered at 1997.2 cm^{-1}, and the *R* branch was centered at 2001.4 cm^{-1} (see Fig. 1). Pump-probe experiments on the *P* branch were performed with the laser centered at 1990.7 and 1992.4 cm^{-1}. Experiments on the *Q* branch were performed with the laser centered at 1997.2 cm^{-1}. Experiments on the *R* branch were performed with the laser centered at 2003 cm^{-1}. The most extensive experiments were conducted on the *Q* branch.

III. RESULTS AND DISCUSSION

A. Spectrum

Gas phase $W(CO)_6$ shows a number of differences from $W(CO)_6$ dissolved in either liquids or supercritical fluids. The infrared spectrum of $W(CO)_6$ in liquids and supercritical fluids are well fit by a single Gaussian. In contrast, the spectrum of gas phase $W(CO)_6$, shown in Fig. 1, has three peaks, the *P*, *Q*, and *R* branches.

The gas phase spectrum of the asymmetric (T_{lu}) CO absorption in a cold $W(CO)_6$ molecule (no vibrations thermally populated and no inhomogeneous broadening) is made up of three series of lines (the *P*, *Q*, and *R* branches). The position of these lines can be described by the following equations.[35]

$$\begin{aligned} P(J)&=\nu_o-(B'_{[\nu]}+B''_{[\nu]}-2B'_{[\nu]}\zeta_i)J+(B'_{[\nu]}-B''_{[\nu]})J^2,\\ Q(J)&=\nu_o+(B'_{[\nu]}-B''_{[\nu]})J+(B'_{[\nu]}-B''_{[\nu]})J^2\\ R(J)&=\nu_o+2B'_{[\nu]}-2B'_{[\nu]}\zeta_i+(3B'_{[\nu]}-B''_{[\nu]}-2B'_{[\nu]}\zeta_i)J\\ &\quad+(B'_{[\nu]}-B''_{[\nu]})J^2, \end{aligned} \tag{1}$$

where $B'_{[\nu]}$ is the rotational constant of the lower state, $B''_{[\nu]}$ is the rotational constant of the upper state, ζ_i is the Coriolis coupling constant for the vibrational mode, and ν_o is the central frequency of the mode. The magnitude of each of the lines is given by the thermal population multiplied by the degeneracy factor $(2J+1)^2$.[35] The Coriolis coupling constant can be calculated from the following equation:[30]

$$\zeta_i=1-\Delta\nu_i\frac{1}{4}\left(\frac{hc}{Bk_BT}\right)^{1/2}=1-\frac{\Delta\nu_i}{3.335(BT)^{1/2}}, \tag{2}$$

where k_B is Boltzmann's constant, $\Delta\nu_i$ is the *P*-*R* branch separation in cm^{-1}, *B* is the rotational constant in cm^{-1}, and *T* is the temperature in *K*. The $B'_{[\nu]}$, $B''_{[\nu]}$, and *B* are calculated through the following equations:[35]

$$\begin{aligned} B&=\frac{h}{4\pi cI},\\ \delta&=\frac{BA}{\nu_0},\\ B'_{[\nu]}&=B-\delta/2.0,\\ B''_{[\nu]}&=B-1.5\delta, \end{aligned} \tag{3}$$

where *I* is the moment of inertia of the molecule, *c* is the speed of light, and *A* is the vibrational anharmonicity, that is, the difference in energy between the 0 to 1 and 1 to 2 transition energies. The anharmonicity for the T_{lu} mode of $W(CO)_6$ is 14.7 cm^{-1}.[36]

For tungsten hexacarbonyl, the calculated value of *B* is 1.97×10^{-2} m^{-1}. The calculated value for δ is 7.3×10^{-5} m^{-1}. The spectrum calculated using the values of *B*, $B'_{[\nu]}$, and $B''_{[\nu]}$, and the experimental temperature, 326 K, is shown in Fig. 2(a). The calculation takes into account the

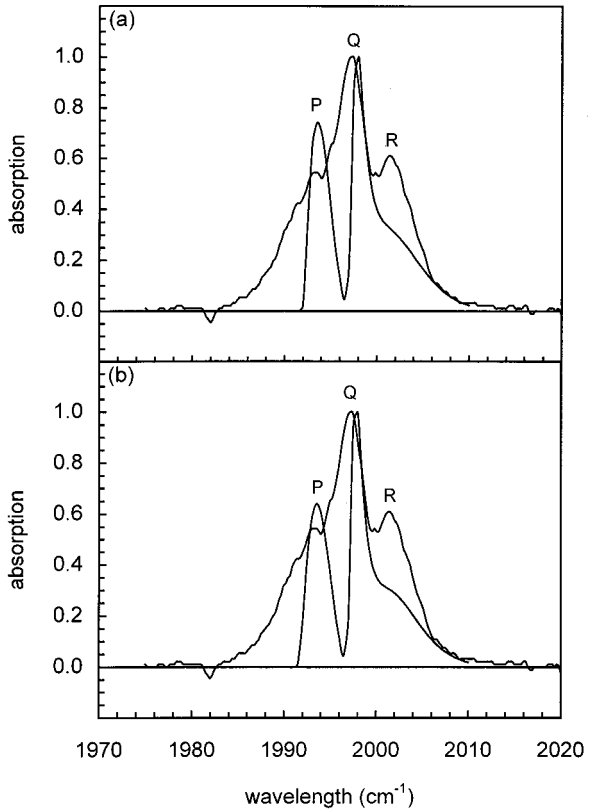

FIG. 2. Calculated spectra taking into account the 0.25 cm^{-1} resolution of the FT-IR, but no other broadening. The experimental spectrum is shown for reference. (a) The calculated spectrum using calculated values of B, $B'_{[v]}$, and $B''_{[v]}$. (b) The calculated spectrum using B and δ as adjustable parameters.

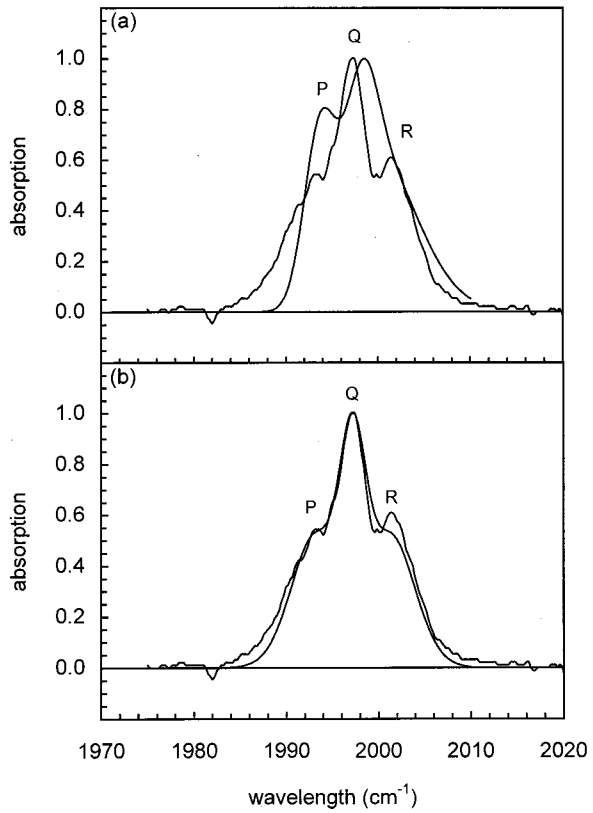

FIG. 3. Calculated spectra including the inhomogeneous width due to "hot band" broadening. The experimental spectrum is shown for reference. (a) The calculated spectrum using σ_{ih} as an adjustable parameter, but using the calculated values of B, $B'_{[v]}$, and $B''_{[v]}$. (b) The calculated spectrum using B, δ, and σ_{ih} as adjustable parameters.

0.25 cm^{-1} spectral resolution of the FT-IR spectrometer used to take the experimental spectra. The amplitude of the calculated spectrum was matched to the experimental spectrum at the peak of the Q branch. The comparison of the calculated spectrum and the experimental spectrum shown in Fig. 2(a) demonstrates that the calculated spectrum does not even qualitatively reproduce the experimental spectrum.

As can be seen from Eq. (3), the values of B, $B'_{[\nu]}$, and $B''_{[\nu]}$ are calculated using the moment of inertia of the molecule. The moment of inertia, however, is calculated assuming that all of the atoms are in a perfectly octahedral geometry. This will not be the case when the sample is at 326 K. The excited low-frequency modes in the molecule will change the bond lengths and bond angles from their low-temperature values. To take this into account, the spectrum was recalculated allowing B and δ to be adjustable parameters. A fit to the experimental spectrum using the adjustable parameters is shown in Fig. 2(b). The fit is not significantly improved.

To fit the spectrum and obtain a reasonable description of the inhomogeneous broadening, an additional width must be added to the spectrum. This broadening is assumed to be Gaussian, and the width (σ_{ih}) is used as an adjustable parameter. The assumption of Gaussian broadening is used for mathematical convenience. As discussed below, the assumption of a Gaussian form for the inhomogeneous broadening may be a source of error in the final calculations. Keeping B and δ fixed at their calculated values and using the Gaussian width of the inhomogeneous broadening (σ_{ih}) as an adjustable parameter, the calculated spectrum is displayed in Fig. 3(a). The peak amplitude of the calculated spectrum was again matched to the peak of the experimental spectrum. The agreement between the calculated spectrum and the experimental spectrum is improved somewhat compared to Fig. 2. As discussed above, however, the values for B and δ assume cold molecules with only the T_{lu} vibrational mode excited. In these high-temperature experiments, however, this is not the case. Using B, δ, and σ_{ih} as adjustable parameters, the fit in Fig. 3(b) is produced. The agreement between the calculated and experimental spectra is greatly improved. While not perfect, when Gaussian inhomogeneous broadening is included in the description of the vibrational-rotational spectrum, a reasonably good description of the experimental spectrum is obtained. The fit in Fig. 3(b) should be compared to the fit in Fig. 2(b), which is the equivalent calculation but without inhomogeneous broadening. The best fit values for the σ_{ih}, B, and δ are given in Table I.

TABLE I. Spectrum fitting parameters [Fig. 3(b)].

σ_{ih}	B	δ
1.47 cm^{-1}	0.0197 m^{-1}	0.0 m^{-1}

The final calculated spectrum is made up of roughly 1000 Gaussians representing J-state transitions up to $J=360$ for each of the P, Q, and R branches. Each Gaussian has a center frequency given by Eq. (1), and a width (standard deviation, σ_{ih}) of 1.47 cm^{-1}. The calculated spectrum is normalized so that the peak corresponds to an absorption of 1, as in the experimental spectrum.

A few obvious sources of this width can be eliminated quickly. The Doppler broadening of the T_{lu} mode in $W(CO)_6$ is only 4×10^{-7} cm^{-1}. The lifetime broadening of this mode is somewhat wider, but still only 4×10^{-3} cm^{-1}.

At 326 K, $W(CO)_6$ has an average of 2900 cm^{-1} of vibrational energy in each molecule. This energy can be arranged in many different combinations of low-frequency modes. In fact, the density of states at this energy (calculated with the harmonic approximation) is 5×10^5states/cm^{-1}.[31,32] As has been pointed out previously,[30] population of low-frequency modes can lead to broadening of the spectrum of a high-frequency mode. This broadening has been referred to in the literature as ''hot band'' broadening.[30]

In the absence of the population of any other modes, the T_{lu} will have a transition frequency, ω_o. If one other mode is excited, then the T_{lu} mode transition frequency will, in general, have a combination band shift, that is, $\omega_o+\Delta_{\lambda,n}$. $\Delta_{\lambda,n}$ is the combination band shift, which can be positive or negative. The subscript λ labels the mode that is excited other than the T_{lu} mode, and the subscript n labels the occupation number of the λth mode. If many modes are excited, then the transition frequency is,

$$\omega_T=\omega_o+\sum\ \Delta_{\lambda,n}, \tag{4}$$

where the sum is over the particular modes excited in a given molecule. (This equation is qualitative because excitation of one mode may influence the combination band shift of another mode.) Because different molecules will have different modes excited with various occupation numbers, there will be a distribution of T_{lu} transition frequencies. The vibrational absorption spectrum for an ensemble of hot molecules in the collisionless gas phase is broadened by the inhomogeneous distribution of occupied modes.

B. Collisionless pump-probe

A typical pump-probe signal in supercritical CO_2 at a density of 2.0 mol/L is shown in Fig. 4.[20] The decay is a single exponential with a decay time of 910 ps. In contrast, as shown in Fig. 5, the decay of the pump-probe signal for the gas phase experiments is a tri-exponential decay with the same decay times, within experimental error, for each branch (P, Q, and R) of the spectrum. The shortest decay time is 140 ps, the middle decay time is 1.3 ns, and the long decay time is greater than 100 ns. The amplitudes of the decay components are dependent on which branch of the spectrum the laser is tuned to, as can be seen in Fig. 5. The major difference among the data sets taken on the different branches is the level of the long time scale ''plateau.''

The amplitude of the decay for the shortest component was approximately the same for the different laser wavelengths, varying between 32% and 35% when fit with a triexponential convolved with Gaussian pump-probe instrument response. The decay amplitude for the middle component depended strongly on the wavelength of the laser (see Fig. 5). For the P branch, the middle component of the decay dropped the signal below the base line by ~10%. In the Q branch experiments, the middle component dropped the signal to a plateau value of ~29%. For the R branch, the middle component dropped to ~48% of the original signal value. The final, long time component has such a long decay time that it appears essentially flat in the data.

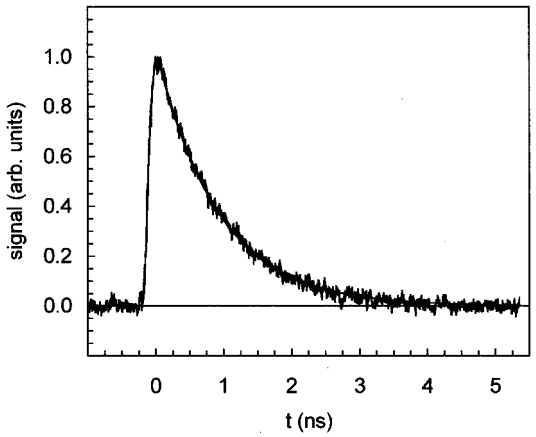

FIG. 4. Pump-probe data taken in supercritical CO_2 at 70 °C with a density of 2.0 mol/L. The decay is a single exponential with a decay time of 910 ps.

From previous density-dependent studies of vibrational energy relaxation of $W(CO)_6$ in supercritical fluids, the zero-density lifetime can be estimated by extrapolation of the density-dependent lifetime data[20] to zero density.[18] The extrapolation is shown in Fig. 6. The spread in the extrapolation comes from making a linear extrapolation using only the lowest density data. From this extrapolation, the lifetime for $W(CO)_6$ in the collisionless gas phase is found to be 1.1 $\pm$0.3 ns. Thus, the middle decay component of the gas phase sample of 1.3 ns can be assigned as the time constant for population relaxation (VER), that is, the relaxation of population out of the initially excited T_{lu} mode. The short time decay is attributed to a spectral diffusion mechanism. The long time decay of the triexponential decays, which appears not to decay on the time scale of the experiment (see Fig. 5), is caused by the change in occupation numbers of the low-frequency modes following population relaxation of the T_{lu} mode.

The fast spectral diffusion term decays to a nonzero constant. The population relaxation term then eliminates the excited state contribution to the signal (one-half of the initial signal). The decay of the excited states produces ground state molecules with increased low-frequency occupation numbers and shifted absorption spectra. This subensemble of spectrally shifted ground state molecules grows in as the excited state population decays. The kinetic equation that describes the signal over the full range of times is

$$S(t)=[R\exp(-k_{sd}t)+(1-R)]\exp(-k_pt) + C[1-\exp(-k_pt)]\exp(-k_lt), \tag{5}$$

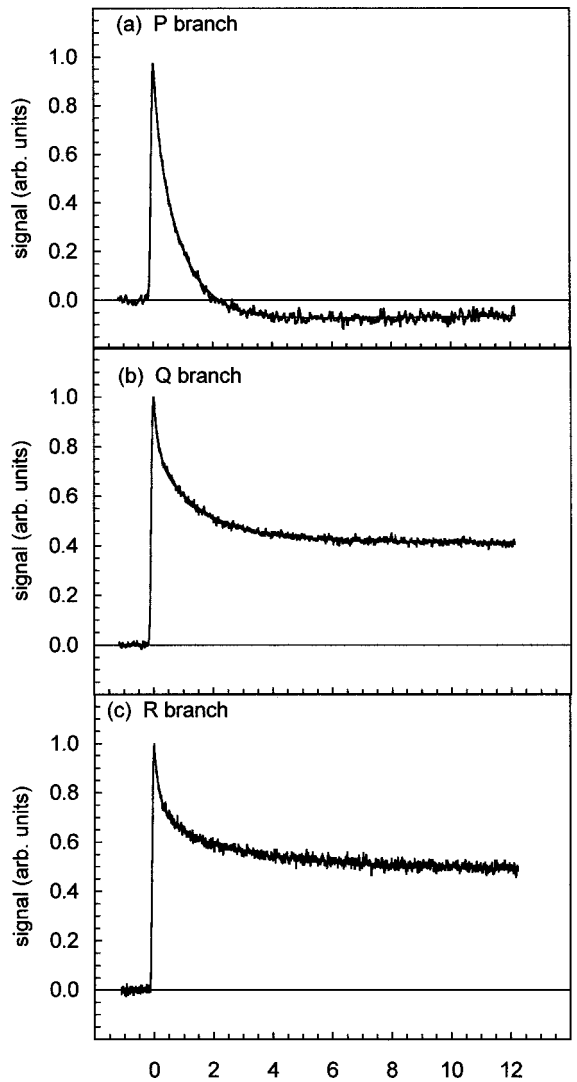

FIG. 5. Pump-probe data on the three branches of the T_{lu} mode. Fits through the data are included, but barely distinguishable. The fit numbers given are averages, after convolution with a Gaussian instrument response. (a) Pump-probe data taken on the *P* branch. The signal decays to 0.10 (arbitrary units) below the base line. (b) Pump-probe data taken on the *Q* branch. The signal decays to 0.29 (arbitrary units) above the base line. (c) Pump-probe data taken on the *R* branch. The signal decays to 0.48 (arbitrary units) above the base line.

where R is the fraction of the signal that disappears due to spectral diffusion, C is the fraction of the signal remaining at long time, k_{sd} is the spectral diffusion (*sd*) rate constant, k_p is rate constant for population (*p*) relaxation out of the T_{lu} mode, and k_l is the rate constant for the very long (*l*) time decay (effectively zero on the experimental time scale).

Equation (5) can be rewritten as

$$S(t)=R\exp[-(k_{sd}+k_p)t]+(1-R)\exp(-k_pt) + C\exp(-k_lt)-C\exp[-(k_p+k_l)t]. \quad (6)$$

This, rigorously, is a tetraexponential decay. However, as long as $k_p \gg k_l$, the equation becomes

$$S(t)=R\exp[-(k_{sd}+k_p)t]+[1-R-C]\exp(-k_pt) + C\exp(-k_lt), \quad (7)$$

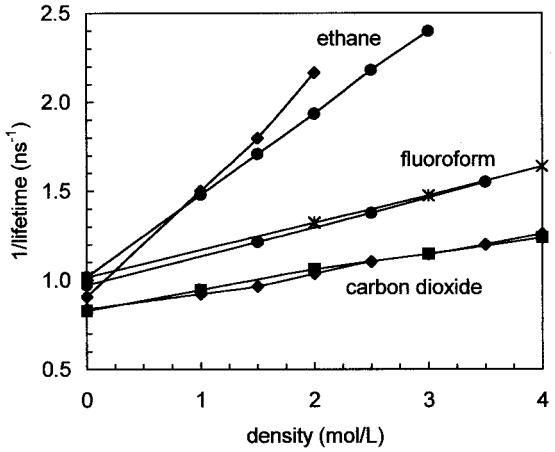

FIG. 6. Vibrational relaxation rate data for the CO asymmetric stretch of $W(CO)_6$ in various supercritical fluids at low densities. Extrapolation of the data to zero density gives an estimate of the gas phase (collisionless) lifetime of ~1.1 ns.

that is, the decay is a triexponential. This is the reason that the data has the appearance of and fits well to triexponential decays (Fig. 5). As can be seen from Eq. (7), the fast rate constant is actually the sum of the spectral diffusion and lifetime rate constants. Since we know the lifetime ($1/k_p = 1.3$ ns), from the observed fast decay time, ~140 ps, we can calculate the average spectral diffusion time ($1/k_{sd}$) to be 157 ps.

Since the laser position and laser bandwidth are known, from the calculated spectrum, the pump-probe signal generated with the laser at a particular wavelength can be calculated. To do this, the excited state population that is generated after the pump pulse interacts with the sample is determined by calculating the overlap of the laser spectrum with each of the individual *J*-state transitions in the IR spectrum as follows:

$$A_{b,j}=\int \exp[-(\omega-\omega_l)^2/(2\sigma_l^2)] \times\exp[-(\omega-\omega_{b,j}^c)^2/(2\sigma_{ih}^2)]d\omega, \quad (8)$$

where b is the branch, j is the *J*-state, ω_l is the laser wavelength, $\omega_{b,j}^c$ is the center (superscript c) wavelength of the particular *J*-state, σ_l is the standard deviation of the laser bandwidth (0.515 cm^{-1}), and σ_{ih} is the standard deviation of the inhomogeneous width (1.47 cm^{-1}). $A_{b,j}$ are the relative populations of the different *J*-states in the excited state. The signal from the excited and ground states cannot be simply calculated from the overlap of the excited state with the probe pulse, however. Any molecule in the excited state is in a particular *J*-state, j'. When it interacts with the probe pulse, the excited state can undergo stimulated emission to either $j'+1$ (the *P* branch), j' (the *Q* branch), or $j'-1$ (the *R* branch). Similarly, the hole in the ground state is not a simple hole, but has *P, Q*, and *R* branches, as well.

Independent of which branch is pumped, the production of excited states produces a stimulated emission spectrum that has three peaks, one in each of the *P, Q*, and *R* branches. The stimulated emission spectrum is what would be ob-

served if the vibrational fluorescence spectrum could be measured. To calculate these stimulated emission peaks, the contribution to each peak from each *J*-transition needs to be determined. Because the laser bandwidth is relatively narrow compared to the inhomogeneous width, the individual *J*-transition contribution to the excited state population is very closely approximated by a Gaussian with the center and width of the laser line. However, the total excited state population produces three peaks in stimulated emission because $\Delta J=0,\pm 1$ downward transitions can be made. At $t=0$, the branch that is pumped has a stimulated emission spectrum that has the center and the width of the laser. The peaks in the other two branches are located within the spectrum of their respective branches, and their widths are broader than the laser because of the differences in the *J*-state separations in the three branches. The amplitudes of the individual *J*-state contributions to the excited state population are calculated by taking the overlap of the particular *J*-transition line shape with the laser spectrum. From the sum of the contribution of each *J*-state, spectra of the peaks in the excited state of each branch can be calculated. The stimulated emission peaks in the *P*, *Q*, and *R* branches at $t=0$ are labeled p_0, q_0, and r_0, and are given by

$$p_0(\omega,t=0)=\sum_j \{A_{p,j}\exp[-(\omega-\omega_{p,j})^2/(2\sigma_l^2)]+A_{q,j-1}\times\exp[-(\omega-(\omega_{q,j-1}-(\omega^c_{q,j-1}-\omega^c_{p,j})))^2/(2\sigma_l^2)]+A_{r,j-2}\exp[-(\omega-(\omega_{r,j-2}-(\omega^c_{r,j-2}-\omega^c_{p,j})))^2/(2\sigma_l^2)]\},$$

$$q_0(\omega,t=0)=\sum_j \{A_{p,j+1}\exp[-(\omega-(\omega_{p,j+1}-(\omega^c_{p,j+1}-\omega^c_{p,j})))^2/(2\sigma_l^2)]+A_{q,j}\times\exp[-(\omega-\omega_{q,j})^2/(2\sigma_l^2)]+A_{r,j-1}\times\exp[-(\omega-(\omega_{r,j-1}-(\omega^c_{r,j-1}-\omega^c_{q,j})))^2/(2\sigma_l^2)]\}, \quad (9)$$

$$r_0(\omega,t=0)=\sum_j \{A_{p,j+2}\exp[-(\omega-(\omega_{p,j+2}-(\omega^c_{p,j+2}-\omega^c_{r,j})))^2/(2\sigma_l^2)]+A_{q,j+1}\exp[-(\omega-(\omega_{q,j+1}-(\omega^c_{q,j+1}-\omega^c_{r,j})))^2/(2\sigma_l^2)]+A_{r,j}\times\exp[-(\omega-\omega_{r,j})^2/(2\sigma_l^2)]\}.$$

Because $t=0$, all of the $\omega_{b,j}=\omega_l$. Figure 7 displays a calculated stimulated emission spectrum using the model spectrum of Fig. 3(b). Also shown is the calculated absorption spectrum (upper curve). In the calculation the hole was taken to be burned at the center of the *Q* branch. As discussed above, the result of hole burning in any branch produces a stimulated emission spectrum with three peaks of differing widths. The spectrum of the hole is the absorption spectrum minus the properly scaled stimulated emission spectrum. The scale factor is determined absolutely by the number of excited states that are created by the pump pulse. (The absolute sizes of the excited state peaks and the ground state holes do not actually enter into the analysis.) Again, the spectrum of the hole consists of three holes, one each in the *P*, *Q*, and *R* branches.

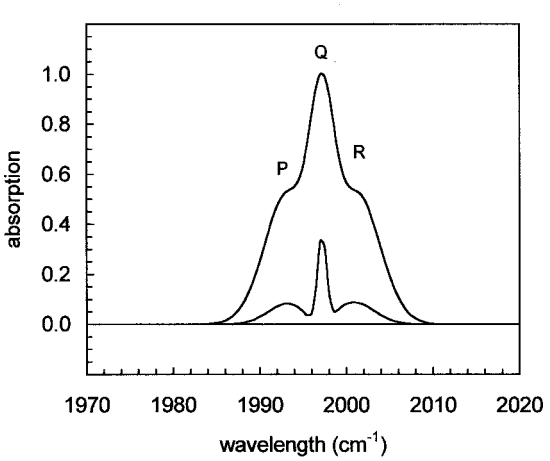

FIG. 7. Stimulated emission spectrum at $t=0$ (lower curve) and the calculated absorption spectrum (upper curve). The spectrum was calculated using the spectrum in Fig. 3(b) with the laser centered on the *Q* branch. The magnitude of the stimulated emission spectrum is greatly exaggerated, as the experiments are carried out at low power.

Following the pump excitation at $t=0$, which produces the initial excited state peak and ground state hole, the spectral diffusion process begins. Spectral diffusion in the excited state causes the excited state peak to broaden. Although its area remains the same (the same number of molecules are excited), less of the area will overlap with the probe pulse spectrum, causing a reduction in stimulated emission. At the same time, spectral diffusion in the ground state causes the hole to broaden (molecules on the outside of the hole move into the hole). Again, although no molecules relax to the ground state, more molecules in the ground state will overlap with the probe pulse spectrum, causing more of the probe pulse to be absorbed. This looks like ground state recovery. It is sufficient to discuss the excited state peak because the behavior of the hole is fundamentally the same.

Inhomogeneous broadening is caused by the distribution of populated low-frequency vibrations. Spectral diffusion is caused by vibrational wave packet dynamics, discussed in more detail below. For a given $t=0$ starting position in the inhomogeneous line, a molecule may be able to sample only a portion of the full range of energies, or it may be able to sample all energies in the inhomogeneous line. For a hole burned off-center, spectral diffusion will broaden the peak and shift it towards the center. For example, if all energies in the inhomogeneous line can be sampled, then the final state should be identical to the entire inhomogeneous line. The peak will have broadened to the full inhomogeneous width and shifted to the center. If only part of the full inhomogeneous distribution can be sampled by the wave packet, then the peak will broaden, but not to the full inhomogeneous width, and it will move toward line center, but not completely. One difference between the excited state peak and the ground state hole is the maximum extent of broadening.

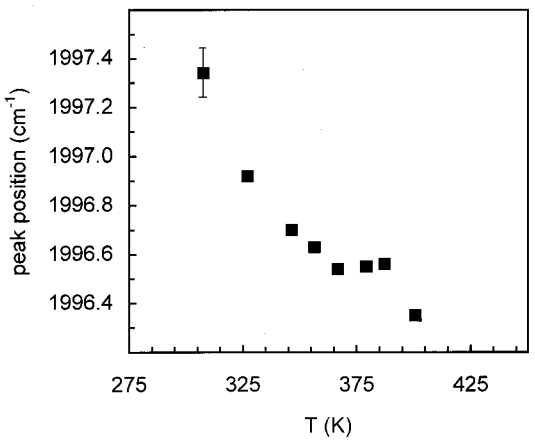

FIG. 8. Absorption frequency (Q-branch) vs temperature for the CO asymmetric stretch of $W(CO)_6$ in the gas phase. A representative error bar is shown. Extrapolation to 450 K (internal vibrational temperature following relaxation of the 2000 cm^{-1} CO stretch if the system was in thermal equilibrium) yields a temperature-dependent shift of ~1.1 cm^{-1} from the peak position at 326 K, the initial sample temperature.

The ground state hole is composed of those molecules that were not excited; they were left in the ground state. Therefore, the maximum broadening is to the full inhomogeneous linewidth. However, the excited state peak is composed of molecules that have a quantum of the T_{lu} mode excited, which they did not have previously. In principle, addition of the T_{lu} excitation changes the vibrational potential for the other modes, which can change their energies and interactions. These changes could modify the inhomogeneous width when the T_{lu} mode is excited, making it possible for the excited state peak to broaden beyond the initial full ground state inhomogeneous width. This possibility is considered below.

To calculate the time dependence of the excited state peak (and ground state hole), both the width (σ) and the center position ($\omega_{b,j}$) of the peak in each J-transition that was initially pumped must change with time. A simple model for the spectral diffusion is assumed. The standard deviation is taken to grow in time to a maximum value. At the same time, the peak moves toward the center at the same rate. The desired time dependence is described by the following equations:

$$\sigma(t)=\alpha-\beta e^{-t/\tau},$$
$$\omega_{b,j}(t)=\gamma-\eta e^{-t/\tau}, \tag{10}$$

where α is the final width, and β is the final width minus the initial width. Similarly, γ is the final frequency, and η is the final minus the initial frequency. In addition, a normalization factor of $(\sigma_l/\sigma(t))$ must be added as a prefactor to the Gaussians so that the areas will remain the same, despite the change in width. Thus, the time-dependent equations for the excited state as it undergoes spectral diffusion in the three branches are

$$\begin{aligned}
p_{sd}(\omega,t)=&\sum_j\left(\frac{\sigma_l}{\sigma(t)}\right)\{A_{p,j}\exp[-(\omega-\omega_{p,j}(t))^2/\\
&(2\sigma^2(t))]+A_{q,j-1}\exp[-(\omega-(\omega_{q,j-1}(t)\\
&-(\omega^c_{q,j-1}-\omega^c_{p,j})))^2/(2\sigma^2(t))]\\
&+A_{r,j-2}\exp[-(\omega-(\omega_{r,j-2}(t)\\
&-(\omega^c_{r,j-2}-\omega^c_{p,j})))^2/(2\sigma^2(t))]\},\\
q_{sd}(\omega,t)=&\sum_j\left(\frac{\sigma_l}{\sigma(t)}\right)\{A_{p,j+1}\exp[-(\omega-(\omega_{p,j+1}(t)\\
&-(\omega^c_{p,j+1}-\omega^c_{q,j})))^2/(2\sigma^2(t))]+A_{q,j}\\
&\times\exp[-(\omega-\omega_{q,j}(t))^2/(2\sigma^2(t))]+A_{r,j-1}\\
&\times\exp[-(\omega-(\omega_{r,j-1}(t)-(\omega^c_{r,j-1}\\
&-\omega^c_{q,j})))^2/(2\sigma^2(t))]\},\\
r_{sd}(\omega,t)=&\sum_j\left(\frac{\sigma_l}{\sigma(t)}\right)\{A_{p,j+2}\exp[-(\omega-(\omega_{p,j+2}(t)\\
&-(\omega^c_{p,j+2}-\omega^c_{r,j})))^2/(2\sigma^2(t))]+A_{q,j+1}\\
&\times\exp[-(\omega-(\omega_{q,j+1}(t)-(\omega^c_{q,j+1}\\
&-\omega^c_{r,j})))^2/(2\sigma^2(t))]+A_{r,j}\\
&\times\exp[-(\omega-\omega_{r,j}(t))^2/(2\sigma^2(t))]\}.
\end{aligned} \tag{11}$$

As discussed above, the time scale for the spectral diffusion (~140 ps) is much faster than the time scale for vibrational population relaxation (~1.3 ns). Therefore, it is sufficient to take the spectral diffusion to be complete on the time scale of the population relaxation. In this case, the initial condition for analysis of the population relaxation is the final state of the system after spectral diffusion is complete.

When the ~2000 cm^{-1} vibrational excitation of the T_{lu} mode relaxes into a distribution of low-frequency modes, the occupation numbers of the low-frequency modes are increased. The increase in the occupation numbers produces a redshift (see below) in the spectrum of the previously excited molecules. Thus, the molecules that are returning to the ground state do not return to the same spectral position as before they were excited. The ground state hole is not changed in this process because the hole is composed of molecules that were never excited. Thus, the ground state hole is the same as it was at the end of the spectral diffusion process. The shift in the absorption spectrum of the molecules that have relaxed from the excited state is responsible for the long time scale decays displayed in Fig. 5.

Because there are no collisions on the time scale of the experiment, all ~2000 cm^{-1} of energy from the T_{lu} mode must go into low-frequency modes of the previously excited molecules. If this energy were to go into a thermal distribution of modes, then the addition of 2000 cm^{-1} to the low-frequency mode occupation numbers would correspond to an increase in temperature of ~125 K (from 326 K to ~450 K) based on calculations using the known mode frequencies and the harmonic approximation for the density of states calculation.[18] Temperature-dependent infrared spectra were

taken of $W(CO)_6$ in the gas phase to determine the amount of shift to be expected from this additional energy.[18] Figure 8 shows the measured Q-branch peak position as a function of temperature. The figure shows that as the temperature is increased, the spectrum redshifts. Extrapolation to 450 K (the internal vibrational temperature following relaxation of the 2000 cm^{-1} CO stretch if the system was in thermal equilibrium) yields a temperature-dependent shift of ~ 1.1 cm^{-1} from the peak position at 326 K, the initial sample temperature.

The spectrum of the molecules that return to the ground state can be modeled in the same way that the excited state spectrum was modeled. The only differences are that the spectrum will be shifted by an amount ω_s and that the width, in the most general treatment, may have changed from the final width following spectral diffusion in the excited state because of the change in the occupation numbers of the low-frequency modes. For times long compared to the exponential population relaxation ($t > \sim 5$ ns), the molecules that have returned to the ground state have shifted (s) spectra, with their P, Q, and R branch shifted spectra labeled p_s, q_s, and r_s, and given by

$$
\begin{aligned}
p_s(\omega, t>5 \text{ ns}) = \sum_j \left(\frac{\sigma_l}{\sigma_s}\right) \{ & A_{p,j} \exp[-(\omega+\omega_s-\omega^f_{p,j})^2/ \\
& (2\sigma_s^2)] + A_{q,j-1} \exp[-(\omega+\omega_s-(\omega^f_{q,j-1} \\
& -(\omega^c_{q,j-1}-\omega^c_{p,j})))^2/(2\sigma_s^2)] \\
& + A_{r,j-2} \exp[-(\omega+\omega_s-(\omega^f_{r,j-2} \\
& -(\omega^c_{r,j-2}-\omega^c_{p,j})))^2/(2\sigma_s^2)]\},
\end{aligned}
$$

$$
\begin{aligned}
q_s(\omega, t>5 \text{ ns}) = \sum_j \left(\frac{\sigma_l}{\sigma_s}\right) \{ & A_{p,j+1} \exp[-(\omega+\omega_s-(\omega^f_{p,j+1} \\
& -(\omega^c_{p,j+1}-\omega^c_{p,j})))^2/(2\sigma_s^2)] \\
& + A_{q,j} \exp[-(\omega+\omega_s-\omega^f_{q,j})^2/(2\sigma_s^2)] \\
& + A_{r,j-1} \exp[-(\omega+\omega_s \\
& -(\omega^f_{r,j-1}-(\omega^c_{r,j-1}-\omega^c_{p,j})))^2/(2\sigma_s^2)]\},
\end{aligned} \tag{12}
$$

$$
\begin{aligned}
r_s(\omega, t>5 \text{ ns}) = \sum_j \left(\frac{\sigma_l}{\sigma_s}\right) \{ & A_{p,j+2} \exp[-(\omega+\omega_s \\
& -(\omega^f_{p,j+2}-(\omega^c_{p,j+2}-\omega^c_{r,j})))^2/(2\sigma_s^2)] \\
& + A_{q,j+1} \exp[-(\omega+\omega_s-(\omega^f_{q,j+1} \\
& -(\omega^c_{q,j+1}-\omega^c_{r,j})))^2/(2\sigma_s^2)] \\
& + A_{r,j} \exp[-(\omega+\omega_s-\omega^f_{r,j})^2/(2\sigma_s^2)]\},
\end{aligned}
$$

where ω_s is the spectral shift following vibrational relaxation, σ_s is the width (standard deviation) of the individual J-transition in the shifted spectrum, and $\omega^f_{m,n}$ is the final spectral position of the nth J-transition of the mth branch.

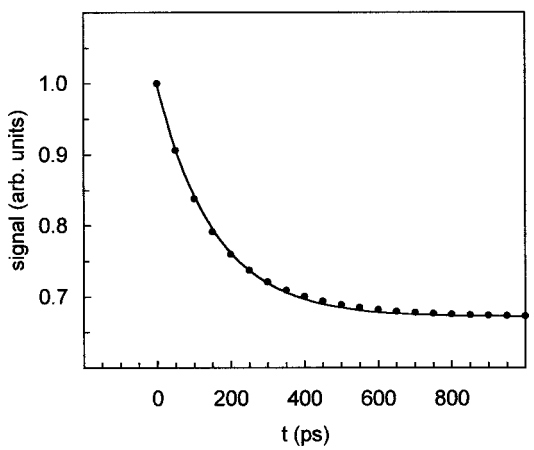

FIG. 9. Comparison of the model calculation to an exponential decaying to a nonzero constant. The decay time of the exponential is 157 ps (the spectral diffusion decay time once the lifetime component is removed). The τ in the model calculation is 208 ps.

To calculate the signal, the overlap of the probe pulse spectrum with the spectrum of the system following excitation must be determined. The overlap (OL) with the probe pulse can be calculated at any time t using

$$
\begin{aligned}
\mathrm{OL}(t) = \int & \exp[-(\omega-\omega_l)^2/(2\sigma_l^2)][p_i(\omega,t)+q_i(\omega,t) \\
& + r_i(\omega,t)]d\omega.
\end{aligned} \tag{13}
$$

The p_i, q_i, and r_i come from Eqs. (9), (11), and (12) for $t=0$, t in the spectral diffusion time range, and $t>5$ ns, respectively. This overlap can now be used to calculate the signal at any time. The general equation for the signal at any time is

$$
\begin{aligned}
S(t) = & \tfrac{1}{2}[\mathrm{OL}_{es}(t)/\mathrm{OL}_{es}(0)] + \tfrac{1}{2}[(\mathrm{OL}_h(t) \\
& - \mathrm{OL}_r(t))/\mathrm{OL}_h(0)].
\end{aligned} \tag{14}
$$

The first term in brackets is the excited state (es) contribution, and the second term in brackets is the ground state depletion contribution. The ground state depletion contribution is the hole (h) minus the excited states that have relaxed (r). The spectrum of the hole is the initial absorption spectrum minus the appropriate excited state stimulated emission spectrum. The spectrum of the relaxed molecules is given in Eq. (12). The $\frac{1}{2}$'s multiplying the terms arise because the signal is comprised of half-stimulated emission from the excited state and half ground state depletion.

The spectral diffusion calculated from Eqs. (11), (13), and (14) does not obviously given an exponential decay of the signal. Figure 9 shows a calculated exponential decay to a nonzero constant (0.67) with a decay time of 157 ps (line), compared to the model's calculated decay (dots). The τ [Eq. (10)] used in the model calculation is 208 ps (this value of τ produces the best fit to the exponential). Although the model calculation does not exactly produce an exponential, the difference is so small that, when included in a triexponential and convolved with a Gaussian instrument response, the difference will not be discernable.

The two models for the spectral diffusion that are considered reflect fundamentally different views of the intramolecular dynamics that give rise to spectral diffusion. In the gas phase, prior to application of the pump pulse, the initial state of the molecule is prepared by its last collision with the wall of the cell or another molecule. The initial state is a complex superposition of low-frequency vibrational eigenstates. Each mode, λ, will have some occupation number, n_λ. Under collision free conditions, for a given molecule, the n_λ are fixed. At the 326 K sample temperature, the average total internal vibrational energy of a molecule is 2900 cm^{-1}, and the density of states at this energy (calculated with the harmonic approximation) is 5×10^5 states/cm^{-1}.[31,32] Thus, there are a vast number of initial states of the molecules that comprise the experimental ensemble.

In model 1, the spectral diffusion is assumed to be produced by wave packet evolution caused by the changing phase relationships among the thermally occupied modes. Following a molecule's last collision prior to the pump pulse, there are well-defined phase relationships among the thermally excited modes. The superposition of these time-evolving vibrational modes produces a complex time-dependent molecular structure. We consider something akin to a Born–Oppenheimer separation of time scales. The 2000 cm^{-1} T_{lu} mode is high frequency compared to the low-frequency modes, which have energies on the order of ~200 cm^{-1}. At a given time, the complex superposition of low-frequency modes projects onto a set of local modes that represent the atomic displacements. In general, the atomic positions will be displaced from their equilibrium average values. The T_{lu} mode is oscillating with a potential determined by the distorted molecular geometry at a particular time. As the wave packet evolves in time, the potential evolves, and the T_{lu} oscillator frequency changes. The change in oscillator frequency is the spectral diffusion. The set of occupation numbers, $\{n_\lambda\}$, and their phase relationships for a particular molecule will produce wave packet evolution that does not necessarily sample the entire inhomogeneous linewidth. The $\{n_\lambda\}$ and their phase relationships will cause the frequency to evolve to some extent about some average frequency. The distribution of the sets of n_λ and the phase relationships determine the distribution of average frequencies. This distribution is the inhomogeneous line. In model 1, the evolution is independent of exciting the T_{lu} mode. Therefore, the spectral diffusion is the same in the ground and excited states. Because the time evolution is independent of the excitation of the T_{lu} mode, the maximum possible extent of spectral diffusion will not exceed the inhomogeneous width that is present prior to vibrational pumping. Also, since the spectral diffusion is not influenced by the excitation of the T_{lu} mode, the extent and rate of spectral diffusion will be the same in the ground and excited states.

In model 2, the spectral diffusion is assumed to be caused by the excitation of the T_{lu} mode. As in model 1, each molecule has a particular $\{n_\lambda\}$, and the inhomogeneous broadening is produced by the distribution of the $\{n_\lambda\}$. When the T_{lu} mode is excited, taking a molecule from the 0 to 1 state of the high-frequency CO stretch, the potentials of the low-frequency modes are changed because of the anharmonic coupling among the modes. Suddenly changing the couplings among the low-frequency modes will cause the initial $\{n_\lambda\}$ to begin to evolve in time. The change in the occupation numbers of the modes induced by vibrational excitation will cause spectral diffusion because the combination band shifts of the T_{lu} mode will change. Because the spectral diffusion is induced by the excitation of the T_{lu} mode, the extent of spectral diffusion could exceed the inhomogeneous width that was present in the ground state prior to the excitation of the high-frequency mode.

In model 2, spectral diffusion only occurs in the excited state. Therefore, the excited state peak produced by the pump pulse broadens, but the ground state hole does not change with time. Broadening of the excited state peak reduces stimulated emission, but because the ground state hole does not fill with time (except for filling caused by the vibrational population relaxation on a longer time scale), changes in the ground state bleach do not contribute to the short time signal decay.

When the equations discussed above are used to model the data, in addition to the time constants for the decays, there are three adjustable parameters. The first is the width over which the excited state can spectrally diffuse, termed the accessible inhomogeneous width. As discussed above, although the transition frequencies are able to evolve in time over a small range, this range is not necessarily the same as the inhomogeneous width, and thus the accessible inhomogeneous width is not necessarily equal to the inhomogeneous width. In the two models discussed, the percentage of the signal remaining after the spectral diffusion process is complete is determined by the accessible inhomogeneous width.

The other two parameters in the calculation of the pump-probe signal are the long time width (the width of the spectrum of the previously excited molecules once they return to the ground vibrational state) and the long time shift of the relaxed molecules. In model 1, all three parameters determine the signal at very long times ($t>5$ ns). In model 2, only the long time width and the long time shift determine the very long time signal, as the hole does not change due to spectral diffusion.

Either model 1 or 2 can describe the full time-dependent decay in the Q branch. For example, consider the decay observed for the Q branch, which is shown in Fig. 5(b). The fit of this particular data set gives a 33.5% drop due to the fast component and a long time component of 35.1%. The decay constants for this particular data set, obtained by fitting to a triexponential, are $k_{sd}+k_p=\frac{1}{155}$ ps for the short time decay, $k_p=\frac{1}{157}$ ns, and $k_l=\sim0$. From the fast decay component, $k_{sd}=\frac{1}{172}$ ps. [Decay times discussed throughout the article, $1/(k_{sd}+k_p)=140$ ps and $1/k_p=1.3$ ns, are average values obtained by fitting many data sets.]

Using model 1 to fit the short time decay component, the accessible inhomogeneous width is 1.043 cm^{-1}, and τ is 232 ps. Once the short time decay has been properly modeled, the accessible inhomogeneous width is fixed, and the long time width and shift are varied to fit the level of the long time decay. To fit the decay shown in Fig. 5(b), the long time width is 1.336 cm^{-1} and the long time shift is 8.0 cm^{-1}. These calculations show that the model is capable of repro-

TABLE II. Results of fits to models 1 and 2 compared to experimental results.

	Laser frequency (cm^{-1})	Measured values	Model 1	Model 2
Accessible inhomogeneous width			0.86 cm^{-1}	2.3 cm^{-1}
Signal after spectral diffusion	1990.7 (*P*)	68%	64%	64%
	1992.4 (*P*)	65%	66%	66%
	1997.2 (*Q*)	67%	75%	74%
	2003.0 (*R*)	67%	65%	63%
Long time width			0.86 cm^{-1}	0.81 cm^{-1}
Long time shift			5.5 cm^{-1}	5.5 cm^{-1}
Long time signal	1990.7 (*P*)	−7%	5%	23%
	1992.4 (*P*)	−11%	6%	23%
	1997.2 (*Q*)	29%	25%	38%
	2003.0 (*R*)	48%	32%	50%

ducing the time-dependent data. The same procedure is used to fit the data using model 2.

Although both model 1 and 2 can fit the *Q* branch data, the true test of the models is their ability to provide a global fit to all of the data taken on the *P*, *Q*, and *R* branches. Both models have reasonable success, but model 1 does a better job. The global fits were made to the average results for the *P*, *Q*, and *R* branches using the procedures described above. A least squares technique was employed to determine the best fit for each parameter. The results from these fits are given in Table II. As discussed above, the time dependence of the data can always be reproduced. However, the magnitude of the decrease in signal produced by spectral diffusion on the short time scale (signal after spectral diffusion) and the long time scale ''plateau'' level (long time signal) are very sensitive to the details of the two models. These signal levels depend on how much spectral diffusion broadens the excited state peak and ground state hole and how much shift there is in the spectrum of molecules after they return to the ground state with 2000 cm^{-1} of excess energy in the low-frequency modes. The column labeled ''laser frequency'' gives the frequency of the pump-probe experiment with the branch of the spectrum in parenthesis. The next column, labeled ''measured values,'' contains the signal levels after spectral diffusion is complete (signal after spectral diffusion) and the signal levels at long time (long time signal). These are the percentages of the signal that remain. The next two columns (models 1 and 2) give the results of the global calculations and the parameters that give the best agreement with the measured values. The first row gives the width following spectral diffusion. The next four rows allow comparison between the data and the calculated results following the spectral diffusion. The rows labeled ''long time width'' and ''long time shift'' give the values of the width and shift of the spectrum of the molecules that have undergone population relaxation to the ground state that produce the best agreement with the data. The four rows labeled ''long time signal'' permit comparison between the measured and calculated values.

From examination of Table II, it is clear that both models reproduce the global behavior of the data qualitatively. For model 1, the spectral diffusion width is less than the full inhomogeneous width, consistent with the model. Model 1 does a reasonably good job of reproducing the signal after spectral diffusion with the exception that the *Q* branch value is somewhat too large. The long time width is the same as that achieved by spectral diffusion and the long time shift is 5.5 cm^{-1}. Model 1 produces the trends seen in the long time data. The two points on the *P* branch have dropped significantly more than the points on the *Q* and *R* branches. However, the drop below zero for the *P* branch is not reproduced and the calculated drop for the *R* branch is too great.

Model 2 does equally well at reproducing the signal after spectral diffusion. A much greater extent of spectral diffusion is required. The width after spectral diffusion is greater than the initial inhomogeneous width. This increased width is permitted in model 2. The long time width is a factor of ~ 3 smaller than the width after spectral diffusion; that is, upon relaxation, the excited state peak must contract to give a shifted narrow ground state peak. The long time width and the long time shift are almost identical to those found in model 1. However, the agreement with the long time signal is not as good for model 2 as it is for model 1. The values for the four experimental wavelengths are very similar. Model 2 can do better at reproducing the *R* branch value, but it does not reproduce the qualitative feature that the signal for the points on the *P* branch show much greater drops than for the *Q* and *R* branches.

The assumptions that the inhomogeneous broadening is Gaussian in functional form and that the form of the time dependence of the spectral diffusion is given in Eq. (10) lead to an exponential time dependence for the spectral diffusion, as shown in Fig. 9. However, as seen in Fig. 3(b), the experimental spectrum is not reproduced perfectly by the Gaussian inhomogeneous broadening model. If the inhomogeneous broadening is not strictly Gaussian or if Eq. (10) does not describe the time dependence accurately, then the time dependence of the spectral diffusion may not be exponential. For example, the time dependence could be a stretched exponential with a fast portion lost underneath the instrument response, which is Gaussian with $\sigma = 37$ ps (FWHM = 87 ps). Any spectral diffusion occurring on a time

TABLE III. Results of fits to model 1 including a very fast component compared to experimental results.

	Laser frequency (cm^{-1})	Measured values	Model 1
Very short time width			0.87 cm^{-1}
Accessible inhomogeneous width			1.25 cm^{-1}
Signal after spectral diffusion	1990.7 (*P*)	68%	64%
	1992.4 (*P*)	65%	67%
	1997.2 (*Q*)	67%	82%
	2003.0 (*R*)	67%	66%
Long time width			1.25 cm^{-1}
Long time shift			5.5 cm^{-1}
Long time signal	1990.7 (*P*)	−7%	−4%
	1992.4 (*P*)	−11%	−7%
	1997.2 (*Q*)	29%	26%
	2003.0 (*R*)	49%	33%

scale faster than the instrument response would not be visible in the experiments. If we assume in the calculations that there is a very fast component to the spectral diffusion that broadens out the excited and ground states in model 1 and just the excited state in model 2, then the results of the model 1 calculations come into closer agreement with the data. For model 2, assuming a fast spectral diffusion component can improve the agreement between the calculations and the spectral diffusion portion of the data but with the result that the long time calculated numbers become much worse, and it is necessary to use physically unreasonable parameters.

Table III displays the results for model 1 when a fast spectral diffusion component is assumed. The first row of the table gives the ''very short time width.'' This is the extent of the very fast spectral diffusion assumed to be lost under the instrument response. The overall accessible inhomogeneous width is increased, but it is still less than the total inhomogeneous broadening obtained from fitting the spectrum. The agreement with the data is improved, particularly in the long time signal. The model is able to reproduce the negative going signals almost quantitatively, which is one of the principal features of the data. However, the calculation still has two places where there is significant deviation from the data, that is, the signal after spectral diffusion for the *Q* branch and the long time signal for the *R* branch. While model 1 with the inclusion of a fast spectral diffusion component gives significantly better agreement with the data than model two, to some extent, the true nature of the phenomena is possibly a mix of model 1 and 2. If both the ground state hole and excited state peak broaden, as in model 1, but there is greater broadening in the excited state, which is characteristic of model 2, then the agreement between experiment and theory could possibly be improved.

One of the important results to come out of these experiments is that the long time shift of the spectrum, regardless of the model, is significantly greater than the estimated 1.1 cm^{-1} shift that would occur from an equilibrium increase in temperature to a final temperature with an average increase in internal energy of 2000 cm^{-1}. Both models indicate a long time shift of 5.5 cm^{-1}. When the T_{lu} mode relaxes into a distribution of low frequency modes, it will not necessary generate a thermal distribution. The T_{lu} mode will relax into a subset of modes that are strongly couple by the anharmonic potential to the T_{lu} mode. These modes will have larger occupation numbers than would be the case in a thermally equilibrated sample. The larger than thermal spectral shift implies that the modes that are strongly coupled to the T_{lu} mode for the purpose of population relaxation also produce large combination band shifts.

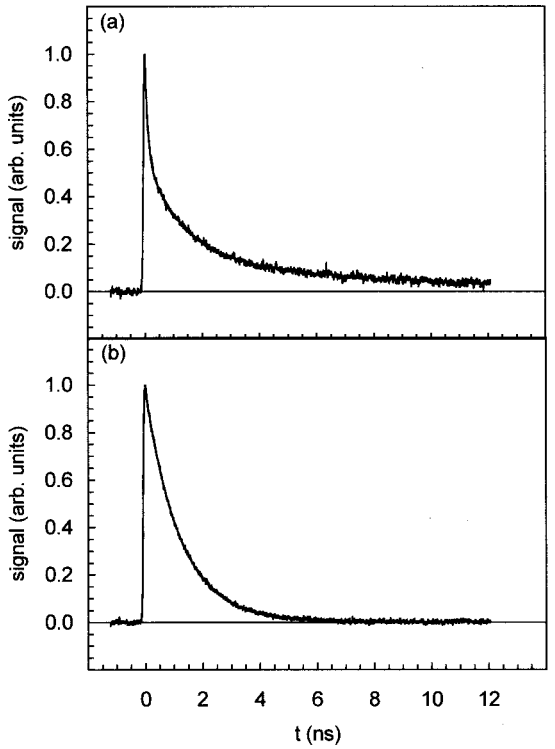

FIG. 10. Sample pump-probe scans on the *Q* branch of the CO asymmetric stretch of $W(CO)_6$ in Ar at two different pressures at 333 K (60 °C). (a) Pressure=18 psi (~1 atm). Ar density of ~ 0.05 mol/L and inverse collision frequency of ~0.2 ns. The decay is fit with tri-exponential components 107 ps, 1.29 ns, and 8.1 ns. (b) Pressure=1180 psi. Ar density of ~3 mol/L. The decay is now a single exponential with a lifetime of 1.20 ns. The average lifetime obtained from several scans is unchanged from the gas phase value, within experimental error.

C. Pump-probe with argon-induced collisions

To see how collisions affect the different decay components, argon was added to the sample at different pressures, and the pump-probe experiments on the *Q* branch were repeated. Figure 10 shows sample pump-probe decay curves when two different pressures of Ar have been added to the sample. Table IV gives the results of fitting the pressure-dependent Ar data at many pressures. At moderate pressure [0.05 mol/L, Fig. 10(a)], the decay remains a triexponential, but the fastest component and the slowest component have become faster (the decays are now 100 ps, 1.29 ns, and 8.1 ns). The lifetime is unchanged within experimental uncertainty. At relatively high pressure of Ar [3.0 mol/L, Fig. 10(b)], the decay is a single exponential. The decay time of

TABLE IV. Fits to pump-probe decays as a function of Ar pressure.

Pressure (psi)	Fast decay time (ps) $(1+k_{sd}+1/k_p)$	Lifetime (ns) $(1/k_p)$	Long decay time (ns) $(1/k_1)$
0.0	140	1.3	>100
0.8	90	1.3	28
2	100	1.0	17
17.8	90	1.2	7.4
50	50	1.1	7.0
100	50	1.1	6.4
250		1.0	4.5
400		1.1	3.6
800		1.0	2.0
1180		1.2	

the single exponential, 1.2 ns, is again, within experimental error, the same as the middle decay component of the triexponential observed without Ar.

In the pressure-dependent data, the long component can distinctly be seen to go from a very long (apparently infinite) decay to a decay that is on the same order as the lifetime. At the highest pressure, a long component can no longer be seen in the data. The short time decay follows a similar trend of increasing rate as the pressure is increased, although the fast component quickly becomes on the same order as the pulse duration, and it can no longer be observed for pressure $\geqslant$100 psi.

The addition of Ar to the $W(CO)_6$ sample increases the rate of collisions. At sufficiently high Ar density, the $W(CO)_6$ molecules are no longer collision free on the time scale of the experiment. As the Ar pressure is increased from zero, the long time decay becomes significantly faster (see Fig. 10). Collisions with Ar provide a mechanism to bring the increased occupation numbers of the low-frequency modes back into thermal equilibrium. Return to thermal equilibrium causes the signal to decay to zero by refilling the ground state hole with the molecules that were spectrally shifted by their increased occupation numbers. At high enough Ar pressures, the long time decay vanishes because the rate of thermal equilibration is fast compared the population relaxation rate.[19] Similarly, as the Ar pressure increases, the spectral diffusion component of the signal gets faster and eventually is no longer observable given the time response of the experiment. Rapid collisions randomize the occupation numbers of the $W(CO)_6$ low-frequency modes producing spectral diffusion that is too fast to observe. Collisions with Ar do not change the population relaxation rate even at relatively high densities. This is in contrast to collisions with polyatomic molecules. For polyatomics, such as ethane, fluoroform, and carbon monoxide, the population relaxation rate is pressure (density) dependent.[19,20] To increase the rate of population relaxation (VER) from its gas phase value, the bath must provide low-frequency modes that enable new relaxation pathways to come into play. Studies of the T_{lu} population relaxation in polyatomic supercritical fluids show that bath modes of $\sim$150 cm^{-1} are required.[19,20] The Ar density of states for the continuum of bath modes cuts off at $\sim$60 cm^{-1}.[37] Therefore, Ar can only enhance vibrational relaxation of the T_{lu} through a multiphonon process, thereby making it ineffective at enhancing the relaxation of the 2000 cm^{-1} T_{lu} mode.

Although Ar is ineffective in causing population relaxation of the high-frequency T_{lu} mode, it is effective at producing population relaxation of the low frequency modes as is evident from Fig. 10 and Table IV. For the pressure in Fig. 10(a) (18 psi, $\sim$1 atm), the inverse collision frequency (hard sphere) is $\sim$0.2 ns. The long component has become substantially faster compared to collision-free conditions and the fast component has also become faster. In Fig. 10(b) (1180 psi), the decay is now a single exponential with lifetime 1.20 ns. The fastest and slowest triexponential components observed in the gas phase are eliminated by rapid collisions with Ar at this high pressure (inverse collision frequency of $\sim$3 ps). The lifetime is unchanged from the gas phase value, within experimental error.

IV. CONCLUDING REMARKS

In this article we have addressed qualitatively and quantitatively the nature of vibrational states and vibrational dynamics in large molecules in the collisionless gas phase at elevated temperatures. The time dependence of the infrared pump-probe experiments on the T_{lu} antisymmetric CO stretch of $W(CO)_6$, a triexponential, has been described as a hole burning experiment. To obtain a reasonable description of the gas phase spectrum, it is necessary to broaden each J to J' transition of the rotational manifolds of the vibrational transition. The inhomogeneous width is $\sim$1.5 cm^{-1}. The inhomogeneous width is associated with the vast number of sets of occupation numbers that the low-frequency modes can have. The different occupation numbers of the low-frequency modes found in different molecules produce different combination band shifts. The distribution of the combination band shifts is the cause of the inhomogeneous broadening.

The bandwidth of the IR pulses is significantly less than the inhomogeneous width. The initial IR excitation burns a hole in the spectrum, creating an excited state peak and ground state hole, initially with the width of the IR bandwidth. The fast component of the triexponential decay arises from spectral diffusion, which can broaden the ground state hole and the excited state peak. The middle component of the triexponential is the T_{lu} mode population relaxation (VER). The very slow component of the decay is caused by the ''heating'' of the low-frequency modes, which produces a spectral shift. The spectral shift prevents the system from returning to the initial conditions until cold molecules fly into the laser spot or infrequent collisions return the system to thermal equilibrium. Addition of Ar produces faster spectral diffusion and faster thermal equilibration. At sufficiently high pressures of Ar, the decay is a signal exponential.

Theoretical analysis of this problem is complex. Two models were presented. Model 1 has both the excited state peak and the ground state hole broaden at the same rate. Model 2 has only the excited state peak broaden. Physical bases for the two models were described. Both models do a reasonable job of reproducing the data. While neither produces complete quantitative agreement with the data, model 1 is somewhat better. Future experiments will test the models

in more detail. In the current experiments, there is a trade off between spectral resolution and time resolution. The future experiments will employ two-dimensional ultrafast infrared stimulated vibrational echo experiments.[38] The stimulated echo can be used to directly examine spectral diffusion on all time scales.

ACKNOWLEDGMENT

This work was supported by the AFOSR (Grant No. F49620-01-1-0018).

[1] R. A. Marcus and N. Sutin, Biophys. Acta **811**, 265 (1985).
[2] R. A. Marcus, J. Phys. Chem. **90**, 3453 (1986).
[3] A. Tokmakoff, M. D. Fayer, and D. Dlott, J. Phys. Chem. **97**, 1901 (1993).
[4] R. G. Gilbert and S. C. Smith, *Theory of Unimolecular and Recombination Reactions*. (Blackwell Scientific, Oxford, 1990).
[5] V. M. Kenkre, A. Tokmakoff, and M. D. Fayer, J. Chem. Phys. **101**, 10618 (1994).
[6] D. W. Oxtoby, Annu. Rev. Phys. Chem. **32**, 77 (1981).
[7] G. Goodyear and R. M. Stratt, J. Chem. Phys. **107**, 3098 (1997).
[8] R. M. Stratt and M. Maroncelli, J. Phys. Chem. **100**, 12981 (1996).
[9] S. A. Egorov and J. L. Skinner, J. Chem. Phys. **105**, 7047 (1996).
[10] S. A. Egorov and J. L. Skinner, J. Chem. Phys. **112**, 275 (2000).
[11] S. A. Egorov, K. F. Everitt, and J. L. Skinner, J. Phys. Chem. A **103**, 9494 (1999).
[12] T. Elsaesser and W. Kaiser, Annu. Rev. Phys. Chem. **42**, 83 (1991).
[13] A. Laubereau and W. Kaiser, Rev. Mod. Phys. **50**, 607 (1978).
[14] A. Tokmakoff, B. Sauter, and M. D. Fayer, J. Chem. Phys. **100**, 9035 (1994).
[15] J. C. Owrutsky, D. Raftery, and R. M. Hochstrasser, Annu. Rev. Phys. Chem. **45**, 519 (1994).
[16] C. B. Harris, D. E. Smith, and D. J. Russell, Chem. Rev. **90**, 481 (1990).
[17] H. J. Bakker, J. Chem. Phys. **98**, 8496 (1993).
[18] D. J. Myers, M. Shigeiwa, R. J. Silbey, and M. D. Fayer, Chem. Phys. Lett. **312**, 399 (1999).
[19] D. J. Myers, M. Shigeiwa, B. J. Cherayil, and M. D. Fayer, J. Chem. Phys. **115**, 4689 (2001).
[20] D. J. Myers, M. Shigeiwa, B. J. Cherayil, and M. D. Fayer, J. Phys. Chem. B **104**, 2402 (2000).
[21] D. J. Myers, S. Chen, M. Shigeiwa, B. J. Cherayil, and M. D. Fayer, J. Chem. Phys. **109**, 5971 (1998).
[22] K. F. Everitt, S. A. Egorov, and J. L. Skinner, Chem. Phys. **235**, 115 (1998).
[23] S. R. J. Brueck and R. M. Osgood, Chem. Phys. Lett. **39**, 568 (1976).
[24] W. F. Calaway and G. E. Ewing, Chem. Phys. Lett. **30**, 485 (1975).
[25] P. Moore, A. Tokmakoff, T. Keyes, and M. D. Fayer, J. Chem. Phys. **103**, 3325 (1995).
[26] *Highly Excited Molecules*, edited by A. S. Mullin and G. C. Schatz (American Chemical Society, Washington, DC, 1997), Vol. 678.
[27] D. J. Myers, M. Shigeiwa, C. Stromberg, M. D. Fayer, and B. J. Cherayil, Chem. Phys. Lett. **325**, 619 (2000).
[28] D. J. Myers, M. Shigeiwa, B. J. Cherayil, and M. D. Fayer, Chem. Phys. Lett. **313**, 592 (1999).
[29] A. Tokmakoff, R. S. Urdahl, D. Zimdars, R. S. Francis, A. S. Kwok, and M. D. Fayer, J. Chem. Phys. **102**, 3919 (1995).
[30] R. S. McDowell and L. B. Asprey, J. Mol. Spectrosc. **48**, 254 (1973).
[31] L. H. Jones, R. S. McDowell, and M. Goldblatt, Inorg. Chem. **8**, 2349 (1969).
[32] D. C. Astholz, J. Troe, and W. Wieters, J. Chem. Phys. **70**, 5107 (1979).
[33] M. Berg, C. A. Walsh, L. R. Narasimhan, K. A. Littau, and M. D. Fayer, J. Chem. Phys. **88**, 1564 (1988).
[34] K. A. Littau, Y. S. Bai, and M. D. Fayer, Chem. Phys. Lett. **159**, 1 (1989).
[35] G. Herzberg, *Molecular Spectra and Molecular Structure II. Infrared and Raman Spectra of Polyatomic Molecules* (Van Nostrand Reinhold C, New York, 1945).
[36] A. Tokmakoff, A. S. Kwok, R. S. Urdahl, and M. D. Fayer, Chem. Phys. Lett. **234**, 289 (1995).
[37] G. V. Vijayadamodar and A. Nitzan, J. Chem. Phys. **103**, 2169 (1995).
[38] D. E. Thompson, K. A. Merchant, and M. D. Fayer, J. Chem. Phys. **115**, 317 (2001).